Finite-element modeling of coupled optical microdisk resonators for displacement sensing

Ivan S. Grudinin* and Nan Yu

Jet Propulsion Laboratory, California Institute of Technology, 4800 Oak Grove Drive, Pasadena, California 91109, USA
**Corresponding author: grudinin@jpl.nasa.gov*

Received August 7, 2012; revised September 11, 2012; accepted September 17, 2012;
posted September 18, 2012 (Doc. ID 174003); published October 3, 2012

We analyze normal mode splitting in a pair of vertically coupled microdisk resonators. A full vectorial finite-element model is used to find the eigenfrequencies of the symmetric and antisymmetric composite modes as a function of coupling distance. We find that the coupled microdisks can compete with the best Fabry–Perot resonators in displacement sensing. We also show how we configured FreeFem++ for the sphere eigenvalue problem.

OCIS codes: 000.4430, 140.4780.

1. INTRODUCTION

In whispering gallery mode (WGM) resonators, the electromagnetic field is trapped inside a circular dielectric by total internal reflections from the boundary [1–3]. Modes of such resonators are distinguished by compact volume and quality factors as high as $Q > 10^{11}$ [4] in a broad range of frequencies. Demonstrated applications of such resonators include microwave cavities for atomic clocks [5], cavity optomechanics [6], nonlinear and quantum optics [7–9], frequency standards [10], biosensors [11–13], microcavity frequency combs [14], RF photonics [15], optical clocks, and ultrastable lasers [16].

When two optical microresonators are placed side by side, the weak evanescent field just outside the surface mediates energy exchange, resulting in optical coupling and normal mode splitting (NMS) [17–19]. The coupled microsphere resonators have been shown to have better displacement sensitivity than sensors based on Fabry–Perot resonators [17]. This sensitivity results from the strong dependence of the NMS of the coupled microtoroid resonators on the gap between the cavities [20]. A further improvement in sensitivity over the edge-coupled configuration was predicted for vertically coupled hemispherical resonators [17]. The experimental realization of such hemispheres has remained unattainable. However, recently developed on-chip microdisk resonators [21] can be fabricated with sufficient control over spectra to make vertically coupled resonator configuration possible.

We here study the NMS of two identical vertically coupled microdisk resonators. Using the finite-element method (FEM) we find NMS for idealized coupled resonator geometries. We also provide a basic noise performance analysis of such displacement transducer.

2. WGM EIGENVALUE PROBLEM WITH FEM

Analytical solutions for WGMs are only available for a limited number of ideal geometries, such as a sphere or an ellipsoid [1–3,22]. The three-dimensional vectorial Maxwell wave equation can be solved numerically, taking the axial symmetry of WGM resonators into account. In this approach [23,24], the problem can be reduced to a system of three coupled equations in a cylindrical two-dimensional "$\rho - z$" section of a resonator. The spurious modes resulting from the improper accounting of the curl operator zero space [25] are partially suppressed by using the penalty coefficient method, enforcing the $\nabla \cdot H = 0$ condition approximately.

We used a scriptable and scalable FreeFem++ solver [26], which utilizes ARPACK [27] for eigenvalue problem solutions. We used UMFPACK [28] as a matrix solver due to its better handling of large matrices compared to other solvers available in FreeFem++. We verify the precision of the FEM approach [24] for the first time as shown in Appendix A.

3. VERTICALLY COUPLED MICRODISK RESONATORS

We used the FEM tool to compute eigenmodes of a pair of vertically coupled microdisk resonators. The computation window with typical resonator geometry is shown in Fig. 1. The figure also shows symmetric (s) and antisymmetric (a) composite modes for TE and TM polarizations [19]. The modes found by the solver were classified as TE or TM by comparing E_z^2 and E_r^2 integrated over the computational window. For TE modes, most of the energy resides in the E_z component.

We investigated the dependence of NMS on the air gap for modes with the wavelength around 1550 nm, with disk radii of $20(M = 10^2)$, $180(M = 10^3)$, and $1750(M = 10^4)$ μm. Since the dependence of NMS on air gap is exponential as expected [17], it was sufficient to only find NMS for two values of the air gap. We adjusted the air gap, keeping the edges of the computational window unchanged. The results are presented in Fig. 2. From the data we obtain the dependence for NMS, $S = 10^{kx+b}$ [GHz] as a function of the gap x [μm] for TM modes, as shown in Table 1. The effective gap [17] characterizing tunability at optical frequency $\nu \simeq 193$ THz is given by $d = \left(\frac{1}{\nu}\frac{\partial S}{\partial x}\right)^{-1} = \left(\frac{1}{\nu}\ln(10)kS\right)^{-1}$.

One observation from Fig. 2 is that compared to silica microtoroids coupled side by side [20], the NMS in vertically coupled microdisks is significantly larger. Another interesting

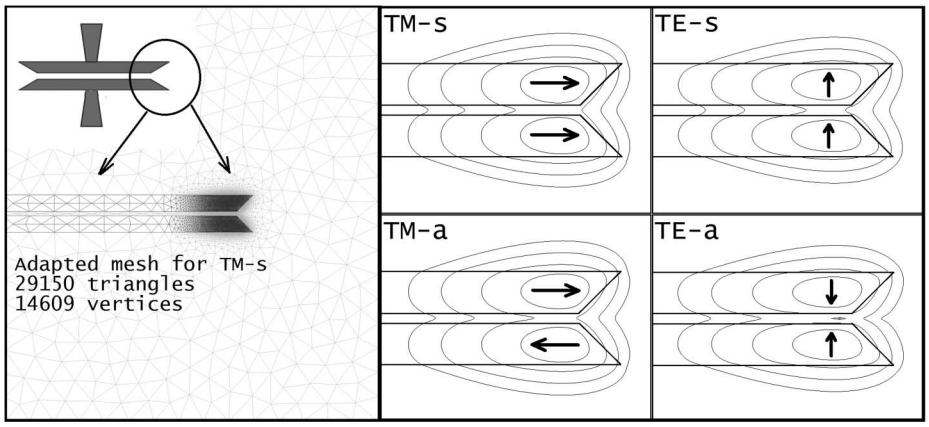

Fig. 1. Vertical coupling of two silica microdisks with refractive index $n = 1.46$, thickness 2 μm, wedge angle 45°, radius 180 μm, air gap 0.5 μm, and the mode orbital index $M = 588$ corresponding to optical wavelength of about 1.56 μm. The amplitude of the magnetic field vector is shown with lines of equal value. From outside, the lines are $H_{\max}/1000$, $H_{\max}/100$,$H_{\max}/10$, and $H_{\max}/2$. Approximate electric field vector directions are shown with arrows.

result is that the mode splitting saturates for large disks: NMS is virtually the same for the disks with radius of 1750 μm as it is for the disks with radius of 180 μm. This may be explained by the increased mode confinement in vertical direction in larger disks. The increased confinement leads to smaller field overlap and coupling. In addition, once the length of the guided WGM exceeds the geometry-specific interaction length [19] the maximum energy exchange has been achieved and no further increase of coupling constant is possible. Indeed, the TM-mode NMS for $M = 1.5 \times 10^4$, $R = 2620$ μm is only 0.2% larger than for $M = 10^4$, $R = 1750$ μm. This indicates that further optimization of disk radius and thickness is possible, which is beyond the scope of this paper. From physical considerations it was expected that vertically coupled configurations will be capable of operating at larger air gaps compared to edge-coupled resonators. Indeed we find that vertically coupled configuration provides NMS similar to coupled microtoroids at roughly double the gap distance. Finally, we observe that the NMS is the largest for the TE modes of smaller disks and for the TM modes of larger disks. This is explained by the influence of the disk wedge. The decrease of the wedge angle is also known to push the mode closer to the disk center; thus we assume that it is mostly equivalent to decreasing the disk's radius.

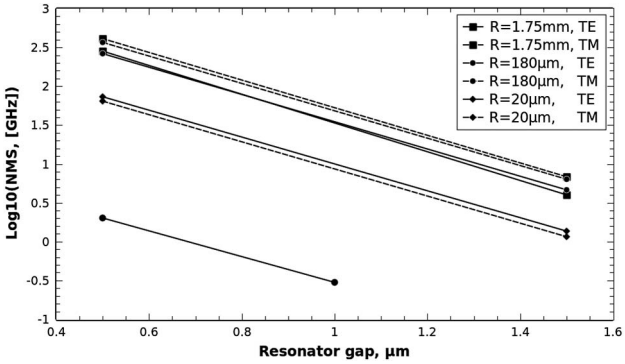

Fig. 2. Mode splitting in vertically coupled microdisks. NMS of silica microtoroids coupled side by side is shown for comparison (adapted from [20]). Error bars are similar in size to point markers and are not shown.

4. DISPLACEMENT MEASUREMENT

For a realistic optical quality factor of $Q = 10^8$ and a pair of resonators separated by a 0.5 μm gap, we obtain the minimum measurable displacement [17],

$$\Delta x = \frac{d}{Q}\sqrt{\frac{h\nu}{W\tau}} = 2.2 \times 10^{-11}\sqrt{\frac{h\nu}{W\tau}}. \quad (1)$$

Here W is the laser power exciting the TM modes having $M = 10^4$. For example, for $W = 100$ μW at 193 THz, and the averaging time of 1 s, the minimum displacement is 8×10^{-19} cm. This value is comparable or better than the sensitivity achievable with the state-of-the-art Fabry–Perot resonators and superconductive microwave cavities. At the same time the on-chip microdisk resonators have small mass of moving parts and can be implemented in a compact measurement setup. For comparison, the effective coefficient of a Fabry–Perot cavity is given by finesse: $d/Q = \lambda/2F$. For state-of-the-art resonators $F \simeq 2 \times 10^6$ [31], giving $d/Q \simeq 3.9 \times 10^{-11}$ cm.

There are a number of factors that can limit the practical sensitivity of the coupled resonator sensor. In addition to photon shot noise, there are such fundamental factors as Brownian and thermorefractive [10,32] noises. One should also avoid the threshold of Kerr and thermal nonlinearity. However, they are specific to a particular NMS measurement scheme and resonator geometries. No nonlinearity was observed for some of the larger microdisks for up to 1 mW of pump power [21]. Thermorefractive noise will be smaller in larger cavities. It was also experimentally found that the Q factor noticeably degraded for the smallest gaps for the coupled toroids [20]. Similarly, it can be expected that the quality factor will depend on the air gap for the vertically coupled disks. It is possible to improve the FEM code to directly compute the radiative Q factor [33] of this system, as will be reported elsewhere.

The ultimate sensitivity of the vertically coupled sensor will depend on the way the NMS is measured. In a passive scheme, laser noise and mechanical noises will determine the sensitivity of the system. One alternative approach is to use an active sensor configuration, where, for example, one of the resonators is doped to provide optical gain. Upon pumping the

Table 1. Displacement Sensitivities of Coupled Microdisks for Optical Frequency around 193 THz (Wavelength 1.56 μm)[a]

Diameter, μm	M	k, μm^{-1}	b	d, cm (at $x = 0.5$ μm)	d/Q, cm
20	10^2	−1.744	2.682	0.075	1.5×10^{-10}
180	10^3	−1.763	3.45	0.013	2.6×10^{-11}
1750	10^4	−1.779	3.507	0.011	2.2×10^{-11}
66	Toroids	−1.647	1.125	2.45	2.45×10^{-7}
Advanced LIGO [29]					1.2×10^{-9}
Capacitive sensor [30]					6×10^{-9}

[a]Typical quality factor is $Q \simeq 5 \times 10^8$ for microdisks and $Q \simeq \times 10^7$ for coupled toroids [20]. The LIGO and the capacitive sensor are listed for reference.

coupled resonators, lasing into normal symmetric and antisymmetric modes will occur (e.g., similar to [34]). The beatnote of the two can be detected with a photodetector, directly providing the NMS. The sensitivity will be limited by the beatnote linewidth, which is in turn limited by the lasing linewidth. While erbium fiber lasers have linewidth less than 10 KHz [35], alternative active schemes may also be used. Finally, it is worth noting that coupled resonators will experience attractive and repulsive forces [36], the magnitude of which can be directly estimated from the tuning curves.

5. CONCLUSION

We have presented a finite-element analysis of the NMS in a system of two vertically coupled silica microdisks. The analysis utilizes a publicly available FEM solver FreeFem++. We find that with the recent advances in microdisk fabrication [21] the vertically coupled resonators have more than two orders of magnitude better displacement sensitivity compared to edge-coupled system. In addition, the sensitivity gain saturates for larger disk diameters. The ultimate displacement measurement sensitivity of this system is comparable to a Fabry–Perot system, while having a much smaller size. The vertically coupled configuration opens new opportunities for scientific and industrial applications of displacement measurements.

APPENDIX A: DIELECTRIC SPHERE AND PRECISION OF FEM RESULTS

We use the well-known weak formulation [24,37] to compute the fundamental TE- and TM- mode frequencies and field distributions in a fused silica sphere with refractive index of 1.46 and azimuthal index $M = 10^3$. We verify the precision of the FEM approach by comparing the solutions to the exact analytical complex eigenvalues that we obtained by numerically solving the following equation in MATLAB [3]:

$$y(Pnh_M^{(1)}(y)j_{M-1}(ny) - j_M(ny)h_{M-1}^{(1)}(y)) + M(1-P)(h_M^{(1)}(y)j_M(ny)) = 0.$$

Here $j_M(ny)$ and $h_M^{(1)}(y)$ are the spherical Bessel and Hankel functions of order M, $y \equiv ka$, a is the resonator's radius, and n is the refractive index. $P = 1$ for TE modes and $P = 1/n^2$ for TM modes. The imaginary parts of the numerical solutions give radiative quality factor of the mode, $Q_{\mathrm{rad}} = \frac{\mathrm{Re}(y)}{2Im(y)}$. A simplified real equation may also be solved, where Hankel functions are replaced with the Neumann function.

We can estimate the error of the FEM solutions as $\delta y = |(y_{\mathrm{fem}} - y_{\mathrm{exact}})|$. The TE and TM solutions are generated on meshes that were adapted to the magnitude of magnetic field vector. The mesh and the mode profile of a TM mode are shown in Fig. 3. The results are shown in Table 2. The absolute frequency error is given by $\delta F = \delta y(c/2\pi a)$. For our mesh this corresponds to around 80 MHz (TE) for a sphere with radius $a = 36$ μm. It shows that the FEM formulation used here, as implemented in FreeFem++, provides good precision for eigenmodes of a sphere. In small microspheres and nonspherical resonators the modes are no longer pure TM and TE, but have hybridized polarizations [33]. Since the weak formulation used here assumes no approximations and models the full field vector, it can be used for arbitrary axially symmetric resonator geometries and is expected to retain good precision. The results obtained with FreeFem++ are very close to those obtained with the commercial package COMSOL Multiphysics, taking into account the lack of easy mesh portability between the two.

While computing the NMS of vertically coupled disks the precision was estimated as follows. For each mode, we started with a homogeneous mesh with approximately 10^4 triangular elements. The mesh was then optimized to the magnetic field

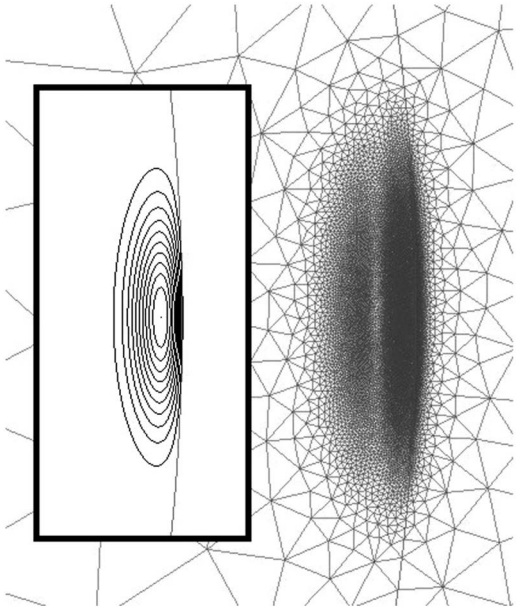

Fig. 3. Adapted mesh in the mode localization region. Inset: FEM solution for a sphere—$TM_{1000,1000,1}$ mode. Iso-value lines are equally spaced, scale for the mesh and the solution is the same.

Table 2. Computed Errors of $y = ka$ for a Sphere[a], $M = 10^3$, $n = 1.46$

	TE	TM
Mesh size[b]	34120/17072	37466/18745
δy	6.2×10^{-5}	7.6×10^{-6}

[a]Second-order Lagrange triangular finite elements were found to provide the best results. Computation required about 2 Gb of memory and 70 s of Intel Core $i7$ 3.2 GHz CPU time. An "electric wall" boundary condition is set on the computational window edges. Sphere radius is $a = 36$ μm, computation window height is 20 μm, left edge is at $a - 8$ μm, right edge is at $a + 5$ μm.
[b]Number of triangles/number of vertices.

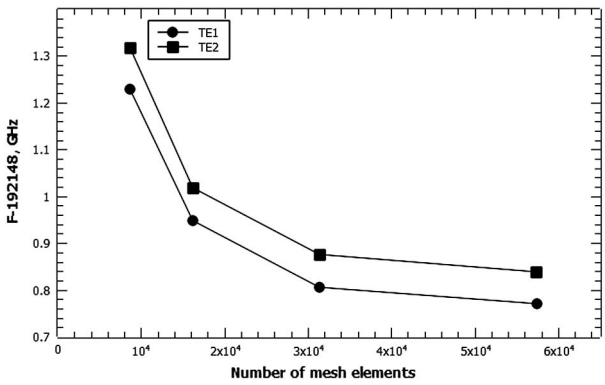

Fig. 4. Convergence of TE composite mode frequencies with increasing number of mesh elements. Vertical axis shows optical frequency offset by 192 THz. Air gap 2.5 μm, $R = 1750$ μm, $M = 10^4$.

vector amplitude of each mode and the new frequency was found. The number of mesh elements was then doubled until reasonable converged solution is achieved. The computation error was chosen as the difference between frequency obtained with the final mesh and that obtained with the previous mesh having half the elements. The mesh refinement was repeated until computation error was less than 0.5 NMS. We observed good convergence of our solutions, as shown in Fig. 4. The computation window edges were also appropriately spaced: the change in frequency due to offset of the walls outwards by 1 μm was much smaller than the computation error of the mode.

ACKNOWLEDGMENTS

This work was carried out at the Jet Propulsion Laboratory, California Institute of Technology, under a contract with the National Aeronautics and Space Administration, with partial support from the NASA Center Innovation Fund and Jet Propulsion Laboratory (JPL) Research and Technology Development Program. We are grateful to K. J. Vahala, M. L. Gorodetsky, R. Thompson, F. Hecht, and participants of the FreeFem mailing list for helpful discussions.

REFERENCES

1. R. D. Richtmyer, "Dielectric resonators," J. Appl. Phys. **10**, 391–398 (1939).
2. A. N. Oraevsky, "Whispering gallery waves," Quantum Electron. **32**, 377–400 (2002).
3. M. L. Gorodetsky, Optical Microresonators with Gigantic Quality Factor (in Russian) (Fizmatlit, 2011), http://www.ozon.ru/context/detail/id/6210477/.
4. A. A. Savchenkov, A. B. Matsko, V. S. Ilchenko, and L. Maleki, "Optical resonators with ten million finesse," Opt. Express **15**, 6768–6773 (2007).
5. R. T. Wang and G. J. Dick, "Cryocooled sapphire oscillator with ultrahigh stability," IEEE Trans. Instrum. Meas. **48**, 528–531 (1999).
6. T. J. Kippenberg and K. J. Vahala, "Cavity opto-mechanics," Opt. Express **15**, 17172–12305 (2007).
7. A. B. Matsko and V. S. Ilchenko, "Optical resonators with whispering–gallery modes—part I: basics," IEEE J. Sel. Top. Quantum Electron. **12**, 3–14 (2006).
8. K. J. Vahala, "Optical microcavities," Nature **424**, 839–846 (2003).
9. J. Moore, M. Tomes, T. Carmon, and M. Jarrahi, "Continuous-wave ultraviolet emission through fourth-harmonic generation in a whispering-gallery resonator," Opt. Express **19**, 24139–24146 (2011).
10. A. B. Matsko, A. A. Savchenkov, N. Yu, and L. Maleki, "Whispering-gallery-mode resonators as frequency references. I. Fundamental limitations," J. Opt. Soc. Am. B **24**, 1324–1335 (2007).
11. C. Shi, H. S. Choi, and A. M. Armani, "Optical microcavities with a thiol-functionalized gold nanoparticle polymer thin film coating," Appl. Phys. Lett. **100**, 013305 (2012).
12. F. Vollmer, S. Arnold, and D. Keng, "Single virus detection from the reactive shift of a whispering-gallery mode," Proc. Natl. Acad. Sci. **105**, 20701–20704 (2008).
13. T. Lu, H. Lee, T. Chen, S. Herchak, J.-H. Kim, S. E. Fraser, R. C. Flagan, and K. Vahala, "High sensitivity nanoparticle detection using optical microcavities," Proc. Natl. Acad. Sci. **108**, 5976–5979 (2011).
14. I. S. Grudinin, L. Baumgartel, and N. Yu, "Frequency comb from a microresonator with engineered spectrum," Opt. Express **20**, 6604–6609 (2012).
15. M. Hossein-Zadeh and A. F. J. Levi, "Ring resonator-based photonic microwave receiver modulator with picowatt sensitivity," IET Optoelectron. **5**, 36–39 (2011).
16. W. Liang, V. S. Ilchenko, A. A. Savchenkov, A. B. Matsko, D. Seidel, and L. Maleki, "Whispering-gallery-mode-resonator-based ultranarrow linewidth external-cavity semiconductor laser," Opt. Lett. **35**, 2822–2824 (2010).
17. V. S. Ilchenko, M. L. Gorodetsky, and S. P. Vyatchanin, "Coupling and tunability of optical whispering–gallery modes: a basis for coordinate meter," Opt. Commun. **107**, 41–48 (1994).
18. V. B. Braginsky, M. L. Gorodetsky, V. S. Ilchenko, and S. P. Vyatchanin, "On the ultimate sensitivity in coordinate measurements," Phys. Lett. A **179**, 244–248 (1993).
19. W. P. Huang, "Coupled–mode theory for optical waveguides: an overview," J. Opt. Soc. Am. A **11**, 963–983 (1994).
20. I. S. Grudinin, H. Lee, O. Painter, and K. J. Vahala, "Phonon laser action in a tunable two–level system," Phys. Rev. Lett. **104**, 083901 (2010).
21. H. Lee, T. Chen, J. Li, K. Y. Yang, S. Jeon, O. Painter, and K. J. Vahala, "Chemically etched ultrahigh-Q wedge-resonator on a silicon chip," Nat. Photonics **6**, 369–373 (2012).
22. M. L. Gorodetsky and A. E. Fomin, "Geometrical theory of whispering-gallery modes," IEEE J. Sel. Top. Quantum Electron. **12**, 33–39 (2006).
23. J. P. Webb, "The finite–element method for finding modes of dielectric–loaded cavities," IEEE Trans. Microwave Theor. **mtt-33**, 635–639 (1985).
24. M. Oxborrow, "Traceable 2-D finite-element simulation of the whispering-gallery modes of axisymmetric electromagnetic resonators," IEEE Trans. Microwave Theor. **55**, 1209–1218 (2007).
25. S. H. Wong and Z. J. Cendes, "Combined finite element–modal solution of three-dimensional eddy current problems," IEEE Trans. Magn. **24**, 2685–2687 (1988).
26. O. Pironneau, F. Hecht, A. Le Hyaric, and J. Morice, "FreeFem++," http://www.freefem.org/.
27. http://www.caam.rice.edu/software/ARPACK/.
28. http://www.cise.ufl.edu/research/sparse/umfpack/.
29. M. A. Arain and G. Mueller, "Optical layout and parameters for the advanced LIGO cavities," LIGO-T0900043-10 (2009).
30. V. B. Braginsky, V. P. Mitrofanov, and V. I. Panov, *Systems with Small Dissipation* (Chicago, 1985).

31. G. Rempe, R. J. Thompson, H. J. Kimble, and R. Lalezari, "Measurement of ultralow losses in an optical interferometer," Opt. Lett. **17** 363–365 (1992).
32. M. L. Gorodetsky and I. S. Grudinin, "Fundamental thermal fluctuations in microspheres," J. Opt. Soc. Am. B **21**, 697–705 (2004).
33. K. Kakihara, N. Kono, K. Saitoh, and M. Koshiba, "Full-vectorical finite element method in a cylindrical coordinate system for loss analysis of photonic wire bends," Opt. Express **14**, 11128–11141 (2006).
34. D. B. Thompson, D. A. Keating, E. Guler, K. Ichimura, M. E. Williams, and K. A. Fuller, "Separation-sensitive measurements of morphology dependent resonances in coupled fluorescent microspheres," Opt. Express **18**, 19209–19218 (2010).
35. B. Wu, Y. Liu, Z. Dai, and S. Liu, "Stable narrow linewidth Er-doped fiber laser at 1550 nm," Microw. Opt. Technol. Lett. **49**, 1453–1456 (2007).
36. M. L. Povinelli, S. G. Johnson, M. Lonar, M. Ibanescu, E. J. Smythe, F. Capasso, and J. D. Joannopoulos, "High-Q enhancement of attractive and repulsive optical forces between coupled whispering gallery-mode resonators," Opt. Express **13**, 8286–8295 (2005).
37. FreeFem++ example is available, http://arxiv.org/abs/1208.4320.